Human General Transcription Factor TFIIB: Conformational Variability and Interaction with VP16 Activation Domain[†]

Fumiaki Hayashi,[‡] Rieko Ishima,[‡] Dingjiang Liu,[‡] Kit I. Tong,[‡] Sungjoon Kim,[§] Danny Reinberg,[§] Stefan Bagby,*,[‡] and Mitsuhiko Ikura*,[‡]

Division of Molecular and Structural Biology, Ontario Cancer Institute, and Department of Medical Biophysics, University of Toronto, 610 University Avenue, Toronto, Ontario M5G 2M9, Canada, and Howard Hughes Medical Institute, Department of Biochemistry, Robert Wood Johnson Medical School, University of Medicine and Dentistry of New Jersey, 675 Hoes Lane, Piscataway, New Jersey 08854-5635

ABSTRACT: Human TFIIB, an essential factor in transcription of protein-coding genes by RNA polymerase II, consists of an amino-terminal zinc binding domain (TFIIBn) connected by a linker of about 60 residues to a carboxy-terminal core domain (TFIIBc). The TFIIB core domain has two internally repeated motifs, each comprising five α-helices arranged as in the cyclin box. Compared to the crystal structure of TFIIBc in complex with TBP and a TATA-containing oligonucleotide, the NMR-derived solution structure of free TFIIBc is more compact, with a different repeat−repeat orientation and a significantly shorter first helix in the second repeat. Analysis of backbone ^{15}N relaxation parameters indicates the presence of relatively large amplitude, nanosecond time-scale motions in the TFIIBc interrepeat linker and structural fluctuations throughout the backbone. Interaction of TFIIBc with the acidic activation domain of VP16 or with TFIIBn induces $^{1}H−^{15}N$ chemical shift and line width changes concentrated in the first repeat, interrepeat linker and the first helix of the second repeat. These results suggest that TFIIB is somewhat pliable and that the conformation of the C-terminal core domain can be modulated by interaction with the N-terminal zinc binding domain. Furthermore, binding of the VP16 activation domain may promote TFIIBc conformations primed for binding to a TBP−DNA complex.

TFIIB is an essential factor for initiation of transcription of protein-coding genes by RNA polymerase II (RNAPII),[1] one of the three eukaryotic nuclear RNA polymerases. Each of these polymerases requires a distinct set of auxiliary protein factors for specific initiation of RNA synthesis. In addition to TFIIB, the general initiation factors for RNAPII are TFIIA, TFIID [TATA binding protein (TBP) is a subunit of TFIID], TFIIE, TFIIF, and TFIIH (*1−4*). In the stepwise model for assembly of a transcription preinitiation complex (PIC) (*1−3*), TFIIB binds to the TBP (TFIID)−DNA complex and acts as a molecular bridge to RNAPII and the remaining initiation factors (*5*). TFIIB possesses sequence-specific DNA binding capacity for a DNA segment termed the IIB recognition element (BRE) immediately upstream of the TATA sequence of the adenovirus major late promoter (*6, 84*). IIB−BRE interaction may play a role in determining the strength of the promoter. PIC formation is completed by binding of RNAPII−TFIIF, followed by TFIIE and finally TFIIH.

Human TFIIB is a 316-residue polypeptide (*7, 8*). Residues 106−316 form a protease-resistant core domain (TFIIBc) (*9, 10*) containing two 76-residue direct repeats which adopt closely similar three-dimensional structures (*11−13*). The solution structure of free TFIIBc (*11*) and the crystal structure of TFIIBc in a TFIIBc−TBP−DNA complex (*12*) differ in repeat orientation. Crystallographic studies of cyclin A (*14, 15*), cyclin H (*16, 17*), and domain A of the retinoblastoma tumor suppressor (*18*) have confirmed a previously predicted (*19*) close structural relationship between TFIIB, cyclins, and the retinoblastoma protein family (*20*). Observation of the same fold in the *Pyrococcus woesei* homologue of TFIIB indicates that the TFIIBc/cyclin box fold evolved before the eukaryotic nucleus (*13*). The protease-sensitive N-terminal 105 residues of human TFIIB include a putative metal binding domain. In the *Pyrococcus furiosus* homologue of TFIIB, the metal binding domain adopts a TFIIS-like zinc ribbon fold (*21*).

* To whom correspondence should be addressed. Phone: (416) 946-2025. Fax: (416) 946-6529. E-mail: sbagby@oci.utoronto.ca; mikura@oci.utoronto.ca.

[‡] Ontario Cancer Institute and University of Toronto.

[§] University of Medicine and Dentistry of New Jersey.

[1] Abbreviations: 2D and 3D, two- and three-dimensional; DTT, dithiothreitol; *E. coli*, *Escherichia coli*; FPLC, fast protein liquid chromatography; HEPES, *N*-(2-hydroxyethyl)piperazine-*N*′-2-ethanesulfonic acid; HSQC, heteronuclear single-quantum coherence; MFA, model-free analysis; NOE, nuclear Overhauser enhancement; NOESY, nuclear Overhauser enhancement spectroscopy; PCR, polymerase chain reaction; PIC, preinitiation complex; QSDF, quasi-spectral density function; RNAPII, RNA polymerase II; TAF, TBP-associated factor; TBP, TATA binding protein; TFIIBc, carboxy-terminal core domain of human TFIIB (residues 1−3 plus 112−316); TFIIBn, N-terminal fragment of TFIIB (residues 1−60); VP16ad, VP16 activation domain (residues 413−490).

RNAPII activity is tightly regulated according to developmental and environmental signals through the interplay of transcriptional activators (*22−24*), repressors (*25, 26*), cofactors (*27*), and the general RNAPII machinery and chromatin (*28, 29*). Activators may function by recruitment of general factors, by inducing conformational changes or covalent modification, and by reducing the repressive effect of chromatin.

Numerous components of the RNAPII machinery have been identified as activator targets. The highly acidic, potent activation domain of the herpes simplex virus type 1 protein VP16 targets TBP (*30*), TFIIB (*31*), and TFIIH (*32*). The VP16 activation domain (*33*) comprises two weaker subdomains, residues 411−456 and 457−490, located at the VP16 C-terminus (*34, 35*). Mutation studies support the role of VP16 in recruitment of TFIIB: mutants that are deficient for activated transcription and interaction with VP16 still support basal transcription (*36*). Biochemical analysis suggests that the N- and C-terminal domains of TFIIB interact, that VP16 induces a conformational change to disrupt this interaction and expose TFIIB functional surfaces (*37*), and that diverse activators recruit TFIIB by a common mechanism (*38*). More recently, the functional significance of TFIIB interaction with VP16 (*39*) and acidic activators in general (*40*) has been questioned. Moreover, VP16 interaction with TBP and TFIIB appeared different in a study using selective excitation of fluorescence: TBP induced greater conformational effects on VP16ad than TFIIB (*41*). Mutation of both TBP and TFIIB showed that transcriptional stimulation by activation domains such as those of VP16 and p53 in human HeLa cells depends on the TBP−TFIIB interaction (*42*). In contrast, the results of a "synthetic lethal" analysis indicated that the TBP−TFIIB interaction is not generally limiting for transcriptional activation in yeast (*43*).

We have exploited the capacity of NMR to characterize both overall and internal protein motions by investigating TFIIBc backbone ^{15}N relaxation. The resulting data are complementary to static studies of structure and indicate the rate and magnitude of any structural fluctuations. Also, to shed light on the mechanism(s) of transcriptional activation involving TFIIB, we have used ^{1}H−^{15}N HSQC spectra to study the interactions between VP16ad and TFIIB and between TFIIBn and TFIIBc. The characteristics of TFIIBc backbone ^{15}N relaxation, including extensive chemical exchange, together with the VP16ad−TFIIB and TFIIBc−TFIIBn interaction data, suggest that TFIIB possesses some conformational pliability.

MATERIALS AND METHODS

Preparation of TFIIBc. Purification and characterization of recombinant TFIIBc, and TFIIBc NMR sample conditions, have been described previously (*11, 44*). The TFIIBc construct used in this study consists of residues 1−3 followed by residues 111−316 of human TFIIB. We performed extensive screening of NMR sample solution conditions before we were able to carry out detailed NMR characterization of TFIIB structure (*11*), dynamics, and interactions. Our screening procedure is described in a separate publication (*45*).

Preparation of TFIIBn. A DNA fragment coding for the N-terminal domain of human TFIIB (Met1 to Ala60) was amplified by PCR using Taq polymerase with pET11b−TFIIB (containing the cDNA for full-length human TFIIB) (*7*) as template DNA. The DNA fragment was generated by the use of a 5′ primer introducing an *Nde*I site (5′-GGAATTC<u>CATATG</u>GCGTCTACCAGCGT) and a 3′ primer introducing a stop codon and *Xho*I site: 5′-GGG<u>CTCGAG</u>T-TATTATGCTTTGTCATTGCTGAAAG. The amplified DNA, coding for TFIIBn, was inserted into pET3a (Novagen) via *Nde*I and *Xho*I sites with expression under the control of the T7 promoter.

Recombinant TFIIBn was expressed in *Escherichia coli* strain BL21(DE3) (Novagen) which contains a chromosomal copy of the T7 RNA polymerase gene under the control of the Lac UV5 promoter (*46*). Cultures were grown at 37 °C in LB medium containing 200 μg/mL ampicillin. Uniformly ^{15}N- and ^{15}N/^{13}C-labeled protein was obtained by using ^{15}NH$_4$Cl and ^{15}NH$_4$Cl/[^{13}C$_6$]-D-glucose as the sole nitrogen/carbon sources in M9 medium. All M9 cultures contained 50 μM ZnCl$_2$. At OD$_{600}$ = 0.8−0.9, TFIIBn synthesis was induced by addition of IPTG to 0.5 mM, and the culture was grown for a further 1.5−2 h. Expression was checked using SDS−PAGE (16% Tricine gels).

Cell paste from a 2 L culture was resuspended in 100 mL of lysis buffer [20 mM Tris-HCl, pH 7.5, 25 mM NaCl, 1 mM DTT, 1 mM PMSF, 30 μM ZnCl$_2$, 10% glycerol, 0.5% NP40, 10 μg/mL DNase I, 3 mM MgCl$_2$, 10 μg/mL pepstatin, 10 μg/mL leupeptin, and 1% (v/v) aprotinin]. The resuspended cell mixture was sonicated using a Branson cell disrupter and then spun down at 27000g for 30 min at 4 °C. The supernatant was loaded onto a DEAE-Sepharose (Pharmacia) column (2.5 × 15 cm). TFIIBn was eluted using a gradient of 25−200 mM NaCl in 20 mM Tris-HCl, pH 7.5, 1 mM DTT, 1 mM PMSF, 30 μM ZnCl$_2$, and 10% glycerol. TFIIBn eluted at 100−125 mM NaCl. Fractions containing TFIIBn were pooled and concentrated to 4 mL using an Amicon ultrafiltration unit fitted with a YM3 membrane filter. The sample was then loaded onto a Sephacryl S100 (Pharmacia) column (2.5 × 88 cm), previously equilibrated with 20 mM Tris-HCl, pH 7.5, 200 mM NaCl, 5% glycerol, 1 mM DTT, 1 mM PMSF, and 30 μM ZnCl$_2$. TFIIBn (approximately 95% pure) eluted at about 270 mL.

Preparation of VP16ad. *E. coli* strain BL21(DE3) harboring the vector pET11cGST.VP16 AD for expression of the C-terminal acidic activation domain of herpes simplex virus activator VP16 (Ala413−Gly490) was grown at 37 °C in LB medium containing 200 μg/mL ampicillin. At OD$_{600}$ = 0.8, protein synthesis was induced by addition of IPTG to 1 mM. The culture was then grown for a further 3 h. Cells were harvested by centrifugation at 4000g.

One hundred milliliters of lysis buffer (20 mM Tris-HCl, pH 7.9, 200 mM NaCl, 10% glycerol, 5 mM MgCl$_2$, 2 mM DTT, 10 μg/mL DNase I, 1 mM PMSF, 10 μg/mL pepstatin, 10 μg/mL leupeptin, 1% (v/v) aprotinin, and 1% Triton X-100) was used to resuspend every 20 g of wet cell paste. Lysozyme (20 mg) was added, and the suspension was incubated, with mixing, at 4 °C for 1 h. The suspension was then centrifuged at 27000g for 30 min. The soluble fraction, containing the GST−VP16ad fusion protein, was loaded onto a 4 mL bed volume column of glutathione−Sepharose (Pharmacia). The column was washed with 100 mL of 20 mM Tris-HCl, pH 7.9, 200 mM NaCl, 1% Triton

X-100, 1 mM PMSF, and 1 mM DTT. The column was then washed, at room temperature, with 50 mL of thrombin cleavage buffer (20 mM Tris-HCl, pH 7.9, 150 mM NaCl, 1 mM DTT, and 2.5 mM CaCl$_2$). The glutathione—Sepharose was then resuspended in 4 mL of thrombin cleavage buffer. To remove GST from the GST—VP16ad fusion protein, 20 units of thrombin (CalBiochem) was added and the glutathione—Sepharose beads were incubated, with mixing, at room temperature for 1 h. Pefabloc (Boehringer Mannheim) was then added to 2 mM to inhibit thrombin activity. VP16ad was eluted with 20 mM Tris-HCl, pH 7.9, 150 mM NaCl, and 1 mM PMSF. The protein, which was about 75% pure at this stage, was lyophilized to dryness and then dissolved in 1 mL of deionized distilled water. The VP16ad solution was loaded onto a Superdex 75 HR FPLC column. The column was run at 0.5 mL/min in 20 mM Tris-HCl, pH 7.5, 250 mM NaCl, 1 mM EDTA, 1 mM DTT, 1 mM PMSF, and 1% (v/v) aprotinin. The recovered VP16ad was about 95% pure. Typically, the yield was about 1 mg of VP16ad/L of LB medium.

NMR Sample Preparation. The NMR sample of ^{15}N-labeled full length human TFIIB comprised 5 mg of protein in 95% H$_2$O/5% D$_2$O containing 20 mM sodium phosphate, pH 7.0, 50 μM zinc chloride, and 5 mM [^{2}H$_{10}$]DTT (Cambridge Isotope Laboratories). The TFIIB—VP16ad sample was prepared by mixing equimolar amounts of ^{15}N-labeled full-length TFIIB and unlabeled VP16ad in the same buffer as that used for ^{15}N-labeled full-length TFIIB alone.

A 0.5 mM sample of ^{15}N-labeled TFIIBc was prepared in 95% H$_2$O/5% D$_2$O containing 10 mM sodium phosphate, pH 6.5, and 5 mM [^{2}H$_{10}$]DTT. The TFIIBc—VP16ad sample was prepared by mixing equimolar amounts of ^{15}N-labeled TFIIBc and unlabeled VP16ad in the same buffer as that used for TFIIBc alone. The TFIIBn—VP16ad sample was prepared by mixing equimolar amounts of ^{15}N-labeled TFIIBn and unlabeled VP16ad in 95% H$_2$O/5% D$_2$O containing 20 mM [^{2}H$_4$]imidazole hydrochloride (MDS Isotopes), pH 6.8, 2.5 mM zinc chloride, 5% glycerol, and 20 mM sodium sulfate. The TFIIBc—TFIIBn sample was prepared by mixing equimolar amounts of ^{15}N-labeled TFIIBc and unlabeled TFIIBn in 95% H$_2$O/5% D$_2$O containing 20 mM [^{2}H$_4$] imidazole hydrochloride, pH 6.8, 2.5 mM zinc chloride, 5% glycerol, and 20 mM sodium sulfate.

NMR Data Acquisition: General. Unless otherwise stated, NMR spectra were acquired at 24 °C on a Varian UNITY-plus 500 spectrometer operating at a proton frequency of 498.260 MHz and equipped with a triple resonance pulsed field gradient probe.

2D ^{15}N-edited HSQC spectra were acquired with the enhanced sensitivity pulsed field gradient approach (*47–50*) and minimized water saturation (*51–54*) with 128 complex points in t_1, 512 complex points in t_2, and 128 transients, except for the spectra of TFIIBc (440 complex points in t_1 and 64 transients) and TFIIBc complexed with VP16ad (160 transients).

Acquisition and Analysis of ^{15}N Relaxation Data. All relaxation experiments were performed at 17 °C using pulse sequences provided by Dr. Lewis Kay (*55*). ^{15}N T_1, ^{15}N T_2, and ^{15}N{^{1}H} NOE experiments for spectral density mapping and model-free analysis (MFA) were performed at 600.289 MHz proton frequency on a Varian Unity 600 spectrometer equipped with a triple resonance pulsed field gradient probe.

The experiments were performed on a 1.2 mM TFIIBc sample and repeated using a 0.6 mM TFIIBc sample to verify that there is no concentration dependence in the relaxation profile. This ensured that the data were not distorted by aggregation.

^{15}N T_1 values were measured from spectra recorded with eight different durations of the delay T: 11.0, 56.0, 111.0, 222.0, 333.0, 444.0, 888.0, and 1776.0 ms. ^{15}N T_2 values were measured from spectra recorded with eight different durations of the delay T: 0.0, 16.0, 32.0, 48.0, 64.0, 80.0, 96.0, and 112.0 ms. To check sample stability, T_2 measurements were repeated with $T = 32.0$ ms after the final acquisition of relaxation data. A recycle delay of 1 s was employed in measurements of both ^{15}N T_1 and ^{15}N T_2 values. ^{15}N{^{1}H} NOE values were determined using spectra recorded in the presence and absence of a 3 s proton saturation period. The NOE experiments were performed three times, and the average values from the three experiments were used.

In addition, ^{15}N T_1 and T_2 were measured using the 1.2 mM sample at 498.260 MHz proton frequency on a Varian UNITY-plus 500 spectrometer. For the ^{15}N T_2 experiment at 498.260 MHz proton frequency, a 3 s recycle delay was required to prevent sample heating. Comparison of the data obtained at 500 and 600 MHz was used to estimate the chemical exchange contribution to T_2 (*56, 57*). Apocalmodulin (*58*) was used as a control (data not shown) to assess the reliability of our data acquisition and analysis.

All relaxation spectra were recorded with 128 complex points in t_1 and 512 complex points in t_2. ^{15}N T_1 and T_2 spectra were recorded with 32 transients per t_1 increment, and ^{15}N{^{1}H} NOE spectra were recorded with 40 transients. Spectral widths of 1800 and 9600 Hz were employed in F_1 and F_2, respectively. The data were processed with nmrPipe (*59*) and analyzed using Pipp (*60*). Lorentzian-to-Gaussian apodization was applied identically to both dimensions of all spectra. T_1, T_2, and NOE values were determined using previously described procedures (*61, 62*). For model-free analysis (*63, 64*), selection and notation of the theoretical relaxation model were as previously described (*65*): 80 cross-peaks were treated by a simplified spectral density function (model I), 6 peaks by the standard Lipari—Szabo function (model II), 10 peaks by a function including two internal motions (model III), 46 peaks by a simplified function incorporating chemical exchange (model IV), and 3 peaks by the standard Lipari—Szabo function including chemical exchange (model V).

RESULTS

TFIIBc ^{1}H–^{15}N HSQC Spectrum. ^{1}H–^{15}N HSQC spectra, representing a fingerprint of the protein backbone, have been used in this study as a quick, informative probe of changes in backbone conformation. Our TFIIBc construct contained 209 amino acid residues, including 10 prolines, 7 asparagines, and 10 glutamines; the expected ^{1}H–^{15}N HSQC peak totals were therefore 198 backbone ^{1}H–^{15}N cross-peaks and 17 pairs of cross-peaks from side chain NH$_2$ groups, plus additional side chain cross-peaks from the 15 lysines and 16 arginines. For the backbone amide groups, 186 resolvable cross-peaks were observed in the HSQC spectrum (Figure 1). Of the non-proline residues, only the first three residues,
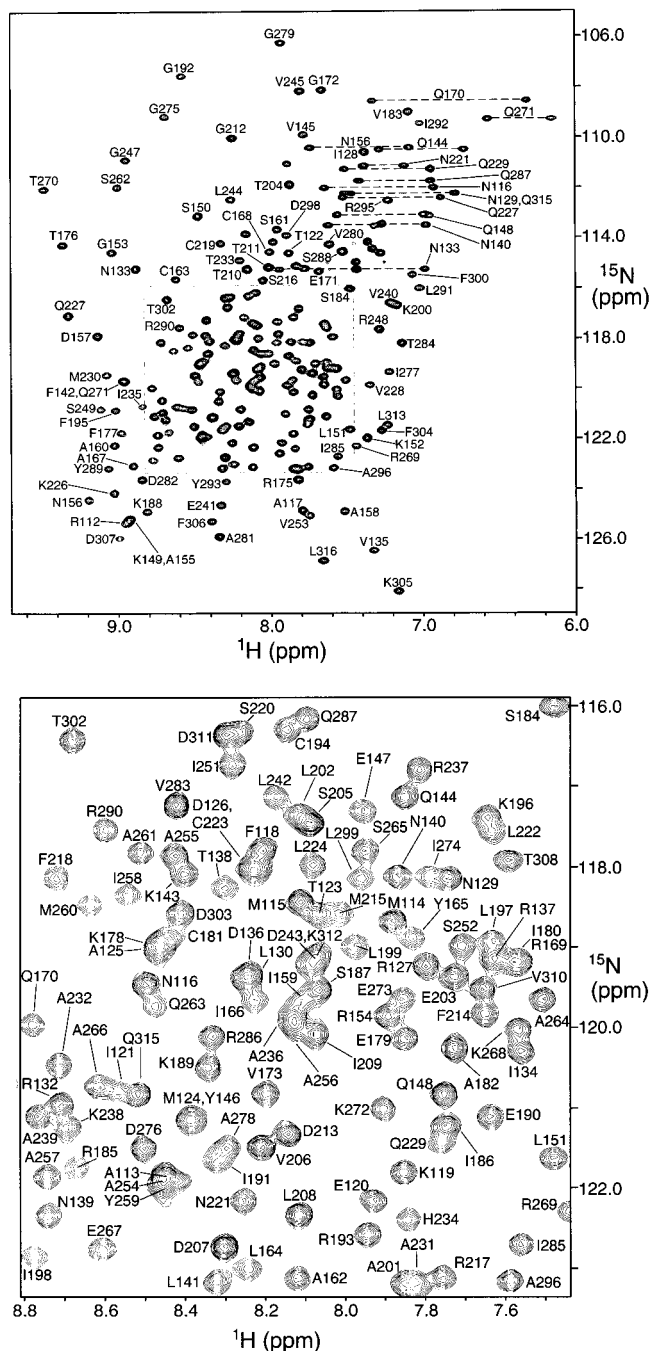
FIGURE 1: (a, top) $^1H-^{15}N$ HSQC spectrum of TFIIBc. The backbone NH group for every residue has been assigned; peaks are labeled according to these assignments using the one-letter amino acid code and sequence position of the corresponding residue. Pairs of peaks connected by dotted lines correspond to asparagine and glutamine side chain NH_2 groups. (b, bottom) Expanded view of the most crowded region outlined using dotted lines in (a, top).

FIGURE 2: Graphical representation of the spectral density functions and model-free parameters of TFIIBc backbone ^{15}N nuclei as a function of residue number, derived from relaxation data recorded at 17 °C, pH 5.8. From top to bottom: (a) $J(0)$; (b) $J(\omega_N = 60$ MHz); (c) $J(\omega_H + \omega_N = 540$ MHz); (d) generalized order parameter, S^2; (e) chemical exchange contribution, R_{ex}, in hertz. Residues for which no results are shown correspond either to proline residues or to residues for which NH cross-peaks could not be resolved. Also shown at the top of the figure is the location of α-helices in the NMR-derived solution structure (*11*) and in the TFIIBc structure in the crystal structure of a TFIIBc−TBP−TATA ternary complex (*12*).

corresponding to residues 1−3 of full-length human TFIIB, did not give any signal in the HSQC spectrum. For asparagine and glutamine side chain NH_2 groups, 14 of the expected 17 pairs of cross-peaks were observed.

Cross-peaks in the $^1H-^{15}N$ HSQC spectrum were reasonably well dispersed, especially considering the relatively large size (23.2 kDa) and helix-dominated secondary structure of TFIIBc. Overlapped backbone NH cross-peaks included those of Arg112, Lys149, and Ala155; Ala113, Ala254, and Tyr259; Met124 and Tyr146; Ala125, Lys178, and Cys181; Asp126 and Cys223; Leu130 and Asp136; Arg169 and
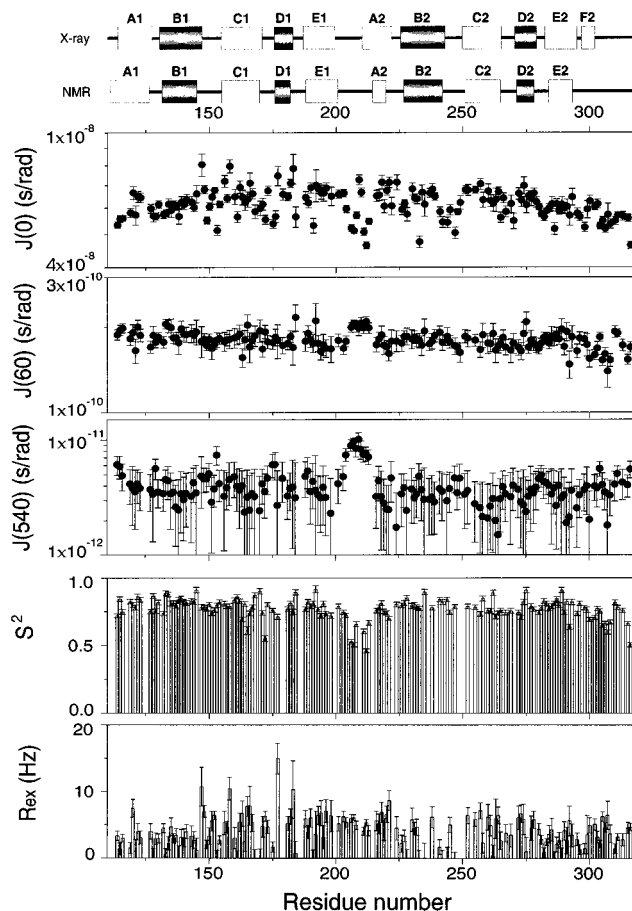
Leu180; and Asp243 and Lys312 (Figure 1b). These cross-peaks were resolved and assigned by analysis of 3D triple resonance spectra.

Backbone ^{15}N Relaxation Studies of TFIIBc. The relaxation parameters T_1, T_2, and $^{15}N\{^1H\}$ NOE for backbone ^{15}N nuclei were obtained by analysis of proton-detected $^1H-$ ^{15}N heteronuclear correlation spectra (*55, 66*). Peak intensities could be estimated for 145 backbone NH groups out of an expected total of 198 cross-peaks. $J(0)$, $J(\omega_N = 60$ MHz), and $J(\omega_H + \omega_N = 540$ MHz) values were calculated by quasi-spectral density function (QSDF) analysis (*56, 67, 68*) (Figure 2). The average values of $J(0)$, $J(\omega_N = 60$ MHz), and $J(\omega_H + \omega_N = 540$ MHz) are 6.16 ± 0.24 ns/rad, 0.181 ± 0.012 ns/rad, and 3.93 ± 1.59 ps/rad. $J(0)$ values are large with an overall convex profile when plotted as a function of residue number, as expected from the concave profile of T_2 as a function of residue number (data not shown). Residues 206−213 in the interrepeat linker have significantly higher $J(\omega_N = 60$ MHz) and $J(\omega_H + \omega_N = 540$ MHz) values than most of the polypeptide, indicating internal motion in the linker on the nanosecond time scale.
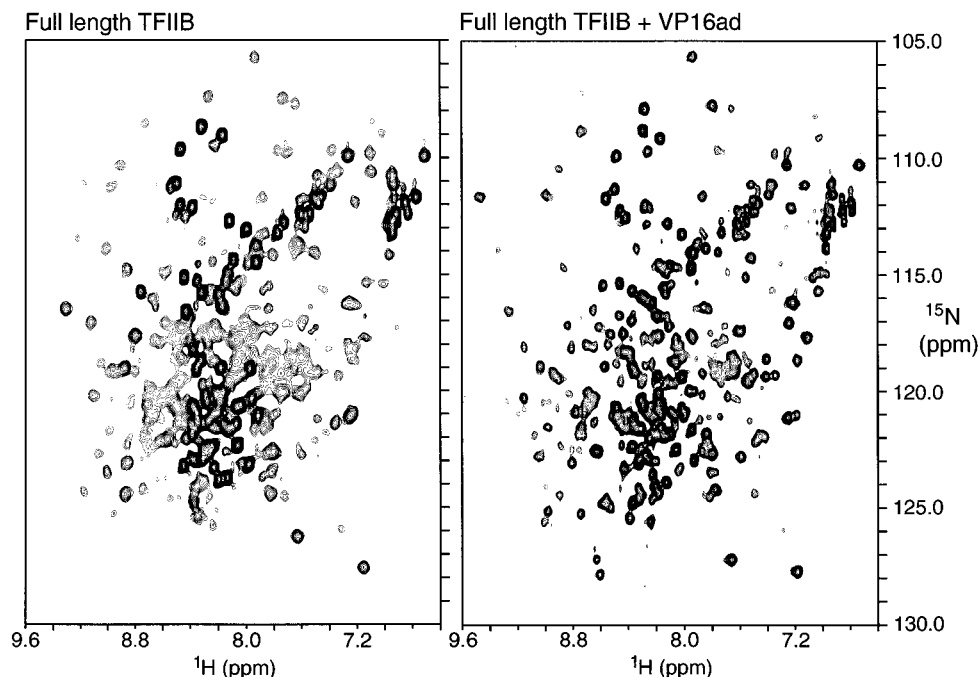
FIGURE 3: $^1H-^{15}N$ HSQC spectra of (a, left) ^{15}N-labeled full-length TFIIB and (b, right) ^{15}N-labeled full-length TFIIB in the presence of 1:1 molar equiv of the unlabeled VP16 activation domain.

To understand the large values and convex profile of $J(0)$, we estimated chemical exchange, R_{ex}, using ^{15}N T_1 and T_2 values measured at 500 and 600 MHz proton frequencies and performed model-free analysis mainly using the data measured at 600 MHz. Comparison of the ^{15}N T_1 and T_2 values at the two field strengths indicated that there is a chemical exchange contribution, R_{ex}, to the apparent rate of T_2 relaxation [and hence to $J(0)$] in most residues of the polypeptide (Figure 2). The R_{ex} values obtained were, however, thought to contain significant error because of the small difference in the field strengths (600 and 500 MHz proton frequency) used for these experiments. Therefore, MFA (*63, 64*) was also performed. For this analysis, we used T_1^{-1}, $^{15}N\{^1H\}$ NOE, and $(T_2^{-1} - R_{ex,min})$, where $R_{ex,min}$ is the minimum R_{ex} contribution for each backbone ^{15}N nucleus obtained by subtracting the maximum error from R_{ex}. $(T_2^{-1} - R_{ex,min})$ contains a residual chemical exchange contribution which can be separated by MFA. The $(T_2^{-1} - R_{ex,min})/T_1^{-1}$ ratio was used to determine an approximate value for τ_R of 16.1 ns. It is noted that the value obtained for τ_R depends on the value assigned to R_{ex}, a quantity with potentially significant error (see above). The generalized order parameter, S^2, also contains this potential error and in this case is an indication of relative internal motion. The generalized order parameter, S^2, and R_{ex} from MFA are shown in Figure 2. Small values of S^2 for residues 206–213 indicate the occurrence of relatively large amplitude motions in the linker between the two repeats, consistent with the observation made for $J(\omega_N = 60 \text{ MHz})$ and $J(\omega_H + \omega_N = 540 \text{ MHz})$.

Interactions between TFIIB and the VP16 Activation Domain and between the N- and C-terminal Domains of TFIIB. Following studies of the structure and dynamics of TFIIBc, we sought direct structural evidence for the proposed (*37*) interaction between the N- and C-terminal domains of full-length TFIIB. Chemical shift overlap and large line widths in the $^1H-^{15}N$ HSQC spectrum of full-length TFIIB

(Figure 3a), however, suggested that detailed structural study would be difficult, if not impossible. On the basis of previous evidence that VP16ad disrupts the proposed intramolecular interaction between the N- and C-terminal domains of full-length TFIIB (*37*), we surmised that investigation of the TFIIB–VP16ad and TFIIBc–TFIIBn interactions could furnish useful insights into TFIIB function. Complexation of ^{15}N-labeled full-length TFIIB with unlabeled VP16ad resulted in a significant improvement in the $^1H-^{15}N$ HSQC spectrum of full-length TFIIB: line widths were reduced by 25% or more, despite the increase in molecular weight upon interaction with VP16ad, and overlap was also reduced (Figure 3b).

Sequential resonance assignments for full-length TFIIB are currently unavailable, so to evaluate the VP16ad interaction surface on TFIIB, and to compare this interaction with that between the N- and C-terminal domains of TFIIB, we recorded $^1H-^{15}N$ HSQC spectra of the following mixtures and monitored changes in chemical shift and line width relative to uncomplexed TFIIBc and uncomplexed TFIIBn.

(1) ^{15}N-Labeled TFIIBc (Residues 111–316) plus Unlabeled VP16ad (Residues 413–490). The $^1H-^{15}N$ HSQC spectrum of TFIIBc in this complex is shown in Figure 4a. Cross-peaks of backbone NH groups showing significant chemical shift changes ($^1H \geq 0.03$ ppm and $^{15}N \geq 0.3$ ppm) and/or line broadening have been boxed. The locations of these NH groups in the TFIIBc structure have been mapped (Figure 5a). Forty-three NH groups in the first repeat of TFIIBc were affected, compared to only 18 in the second repeat. Clusters of affected residues occurred in helix C1 at the center of the first repeat and in basic amphipathic helix E1. Interestingly, the NH groups of 5 residues in the linker, 3 in helix A2, and 14 other residues at the interface between the repeats showed significant changes upon VP16ad binding.

(2) ^{15}N-Labeled TFIIBc (Residues 111–316) plus Unlabeled TFIIBn (Residues 1–60). The $^1H-^{15}N$ HSQC spectrum of ^{15}N-labeled TFIIBc in this complex is shown in
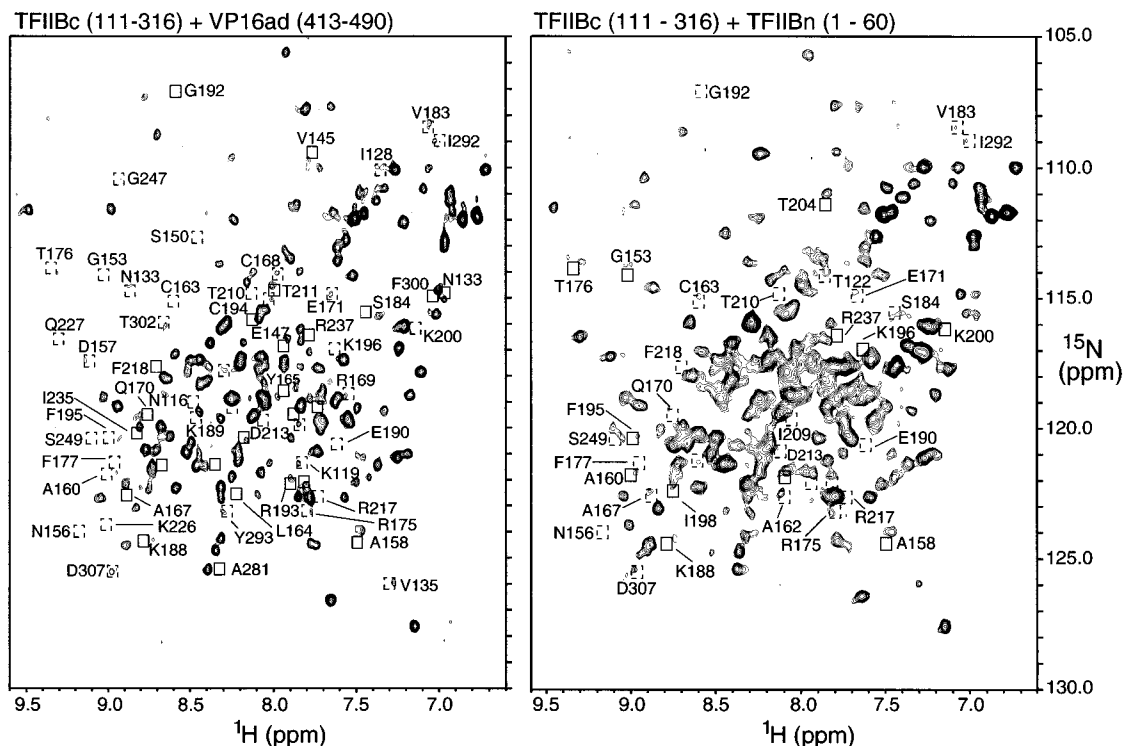
FIGURE 4: ^{1}H$-^{15}$N HSQC spectra of (a, left) ^{15}N-labeled TFIIBc in the presence of 1:1 molar equiv of unlabeled VP16ad and (b, right) ^{15}N-labeled TFIIBc in the presence of 1:1 molar equiv of unlabeled TFIIBn. A box with a broken outline indicates line width change relative to the ^{1}H$-^{15}$N HSQC spectrum of TFIIBc alone, and a box with a solid line indicates a chemical shift change or evidence of both line width and chemical shift change. Where cross-peak density permits, cross-peaks that show significant chemical shift and/or line width changes relative to the ^{1}H$-^{15}$N HSQC spectrum of TFIIBc alone are labeled with the one-letter amino acid code and sequence position of the corresponding amino acid residue.

Figure 4b. Cross-peaks of backbone NH groups showing chemical shift changes and/or line broadening (boxed in Figure 4b) have been mapped onto the structure of TFIIBc (Figure 5b). As observed with VP16ad, most (twenty-five) of the significantly affected NH groups mapped to the first repeat of TFIIBc. Helices C1, D1, and E1 showed most change. Again, five linker residues and two in helix A2 were affected. Apart from helix A2, only four backbone NH groups in the second repeat were affected.

(3) ^{15}N-Labeled TFIIBn (Residues 1−60) plus Unlabeled VP16ad (Residues 413−490). The ^{1}H$-^{15}$N HSQC spectrum of TFIIBn was not significantly affected by mixing with VP16ad. This suggests either that the two polypeptides did not interact or that VP16ad binding did not alter the conformation of TFIIBn.

DISCUSSION

The solution structure of unbound human TFIIBc (*11*) and the crystal structure of TFIIBc determined in complex with *Arabidopsis thaliana* TBP2 and the TATA element of the adenovirus major late promoter (AdMLP) (*12*) differ in two related respects: the relative orientation of the domains formed by the first and second TFIIBc repeats (Figure 6) and the lengths of the interrepeat linker and first α-helix of the second repeat (helix A2 in the NMR structure, helix BH1′ in the crystal structure; Figures 6 and 7). The folds of the individual repeats are similar in the crystal and solution structures. Helix A2 in the TFIIBc solution structure comprises only 5 residues (Figure 7), but is 12 residues long in the TFIIBc−TBP2−TATA complex crystal structure (*12*) (Figure 6c). Helix A1, the first repeat helix corresponding

to helix A2, is 15 residues long in solution, close in length to its ternary complex counterpart.

In the solution structure of free TFIIBc, the repeat interface occurs in the region comprising helices C1, D1, C2, and D2: the C1−D1 loop is close to the C2−D2 loop and helix D2 (Figure 6), with a buried surface area between the domains of approximately 1500 Å^2. In the TFIIBc structure taken from a TFIIBc−TBP−DNA ternary complex (Figure 6), the repeat interface occurs between the C1−D1 loop and helix A2 and between helix D1 and the D2−E2 loop (Figure 6). The aforementioned considerably shorter length of helix A2 in free TFIIBc compared to that in the TFIIBc−TBP− DNA complex is compatible with the domain orientation observed in free TFIIBc, where helix A2 is not part of the domain interface but rather is solvent exposed and therefore lacks stabilizing interactions. The buried surface area between the TFIIBc repeats in the complex crystal structure is 600 Å^2 (*12*). The structure of unbound TFIIBc in solution is thus more compact than that of TFIIBc bound to a TBP− DNA complex in the crystalline state (54 Å × 33 Å × 35 Å for the solution structure and 65 Å × 32 Å × 32 Å for the crystal structure). Residues involved in NOEs that define the relative orientation of the first and second repeat motifs include Glu172, Pro174, Arg175, Phe195, Ser262, Gln263, Arg269, Ile274, Arg286, and Leu313. NOEs between the TFIIBc repeats that might be expected on the basis of the repeat orientation observed in the ternary complex crystal structure involve Arg175, Thr176, and the aromatic rings of Phe214 and Phe218. Such NOEs were not observed in our spectra of unbound TFIIBc in solution. We note the different conditions used for NMR and X-ray crystallography: TFIIBc
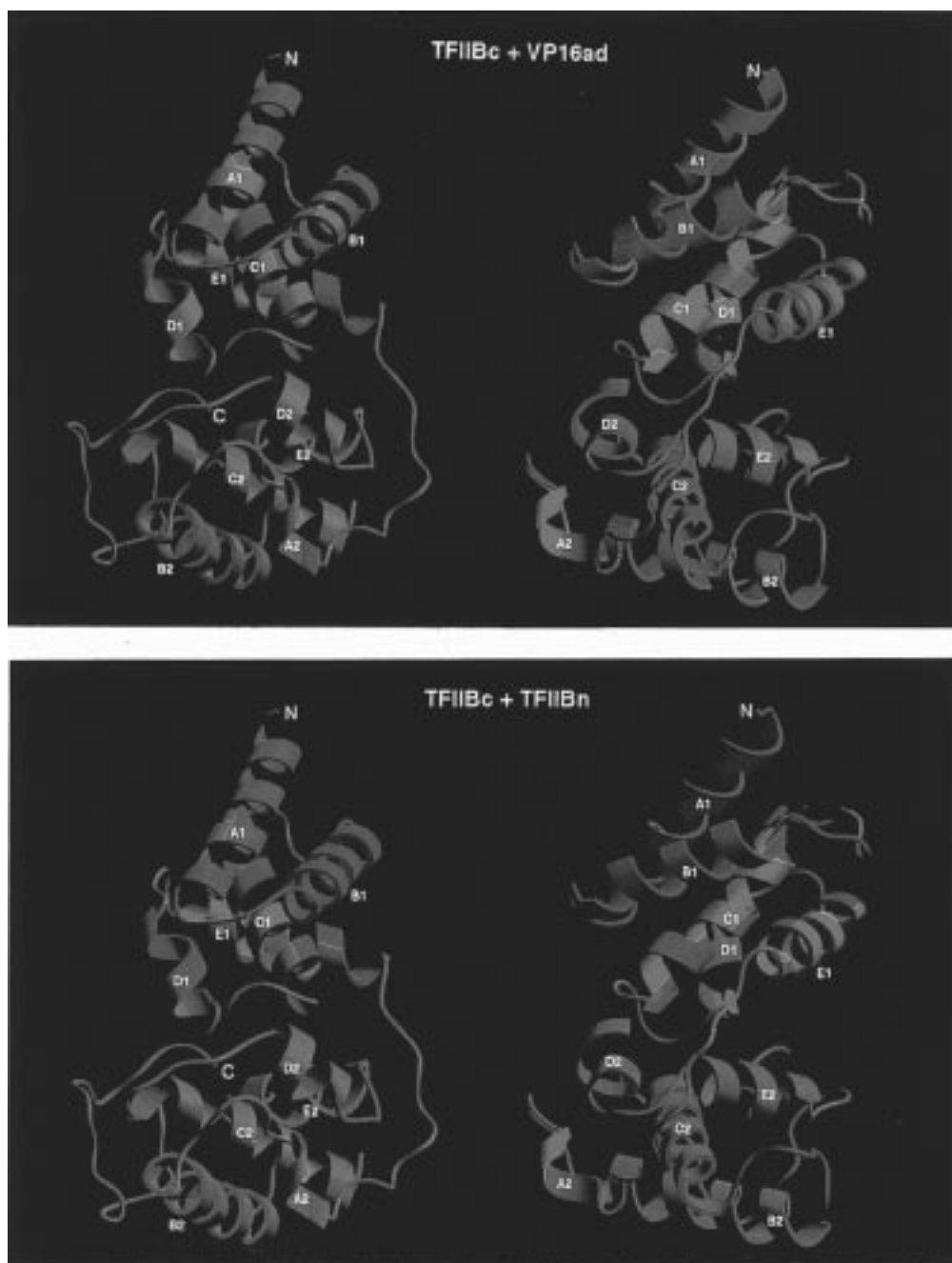
FIGURE 5: Effects of (a, top) VP16ad and (b, bottom) TFIIBn mapped onto the structure of TFIIBc. The first repeat of TFIIBc is shown in green and the second repeat in cyan, and the location of NH groups corresponding to shifted/broadened cross-peaks is indicated in red.

samples used for acquisition of NMR spectra contained 10 mM sodium phosphate, pH 5.8, 7.5 mM perdeuterated dithiothreitol, and 50 μM sodium azide (*11*); the TFIIBc—TBP—DNA complex used for crystallographic studies (*12*) was prepared in 40 mM KCl, 300 mM ammonium acetate, 5 mM $MgCl_2$, 5 mM $CaCl_2$, 10 μM zinc acetate, 10 mM dithiothreitol, 10% (v/v) glycerol, 2% (v/v) ethylene glycol, and 40 mM Tris-HCl, pH 8.5, and was crystallized by vapor diffusion against 5—10% (v/v) glycerol, 20 mM dithiothreitol, and 40 mM Tris-HCl, pH 8.5.

The difference between the structures of free and complexed TFIIBc lead us to investigate the potential for structural fluctuations in TFIIBc through examination of backbone ^{15}N dynamics of free TFIIBc in solution. Such an investigation of dynamics requires measurement and analysis of relaxation times and heteronuclear NOEs. The

relaxation data indicate distinctive behavior in the linker between the two repeats and the presence of chemical exchange throughout TFIIBc. The spectral density maps at 60 and 540 MHz indicate the presence of internal motion in the linker on a nanosecond time scale. Moreover, the spectral density function at zero frequency, $J(0)$, dips in this part of the TFIIBc sequence due to internal motion (Figure 2). This motion produces a longer T_2 by more effective averaging of dipolar interactions. After removal of the minimum chemical exchange contribution, MFA (*63, 64*) produces a similar conclusion: the relatively low values of the order parameter, S^2 (Figure 2), and the correlation time for internal motion, τ_e, in the linker evidence relatively large amplitude motions on a nanosecond time scale. It should also be noted that variant linker conformations sometimes occurred in an ensemble of NMR-derived structures (data not shown). In
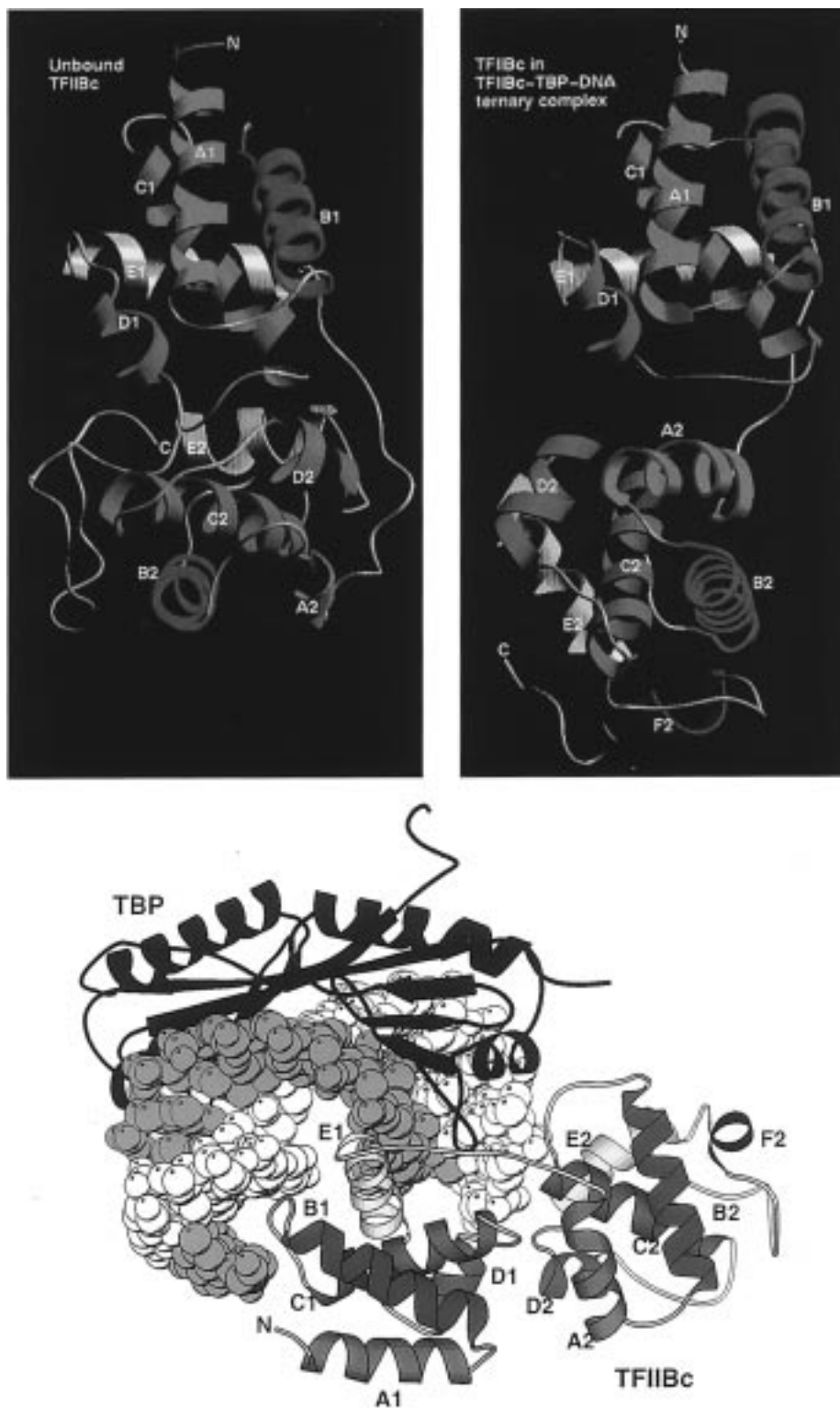
FIGURE 6: Relative orientation of the repeat motifs in (a, top left) the NMR-derived solution structure of unbound TFIIBc and (b, top right) the X-ray crystallographic structure of TFIIBc taken from a ternary TFIIBc−TBP−TATA complex. Backbone atoms of residues 112−199 of the coordinates of unbound and complexed structures were best-fitted for this figure. Note the markedly different lengths of the first helix of the second repeat (helix A2) in the two structures. NMR data for helices A1 and A2 are compared in Figure 7. (c, bottom) The TFIIBc−TBP−TATA ternary complex crystal structure (*12*). The color scheme used for the TFIIBc helices in (a) and (b) is retained in (c). TBP is shown in dark blue, and the strands of the TATA element are shown in orange and white (space-filling representation).

the crystal structure of bound TFIIBc, residues 211−213 are part of the first helix of the second repeat and are located in the domain interface. Our backbone ^{15}N relaxation data indicate that the backbone amides of these residues are mobile, more consistent with their solvent-exposed location in the NMR structure of free TFIIBc (Figure 6).

$J(0)$ displays large, scattered values within an unusual convex overall envelope. At least some of the unusual character of $J(0)$ can be ascribed to the widespread chemical exchange contribution to T_2 relaxation. TFIIBc in solution has a somewhat elongated shape with diffusion axes in the ratio 1:1.03:1.75. Anisotropy of molecular diffusion was not
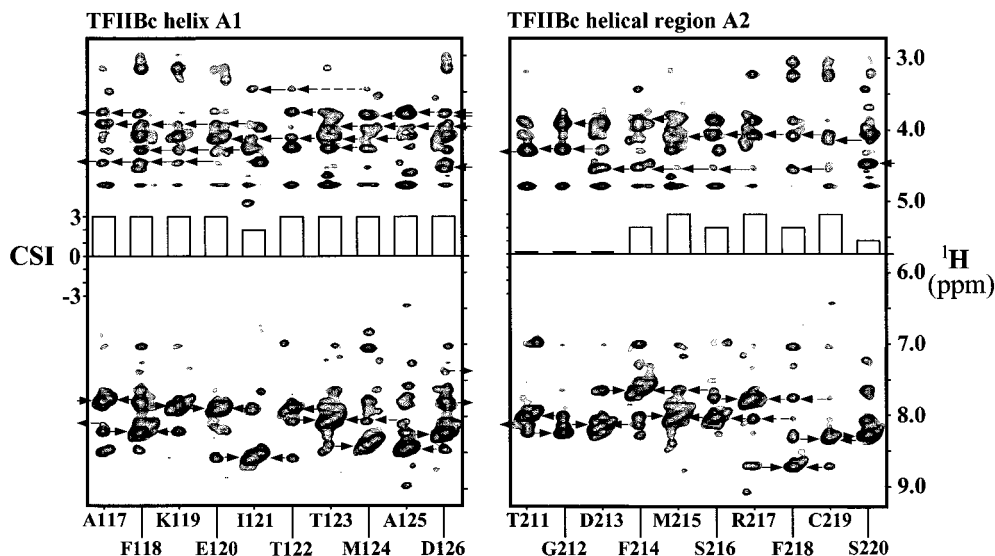
FIGURE 7: Chemical shift indices and sequential and short-range backbone NOEs for the first α-helix in each of the repeats of TFIIBc to illustrate the evidence for the significantly different lengths of these helices. The strip plots were extracted from a ^{15}N-edited NOESY−HSQC spectrum of TFIIBc.

incorporated into our analysis, however, since there was no correlation between the T_1/T_2 ratio and the projection of the NH bond vector onto the diffusion axis. In the absence of evidence for two or more rotational correlation times, therefore, a single rotational correlation time has been assumed, with attribution of short T_2 values to chemical exchange. Also, chemical exchange and anisotropy may be interrelated in the sense that any conformational exchange correspondingly results in transient changes in molecular anisotropy.

There are few published examples of proteins that show such widespread chemical exchange. Examples include the isolated N-terminal SH3 domain of Drk (69, 70), the C-terminal domain of apocalmodulin (58), and unliganded FK506 binding protein (71). We identified three specific structural properties of TFIIBc that might be related to widespread chemical exchange: (1) most pairs of β-CH$_2$ protons have degenerate chemical shifts (approximately 60% are degenerate in the N-terminal repeat and approximately 80% are degenerate in the C-terminal repeat), (2) the TFIIBc repeats have a small hydrophobic core, and (3) some parts of the H/D exchange data do not correlate well with the solution structure. Degenerate chemical shifts of β-CH$_2$ protons suggest that the side chains can rotate freely and that the hydrophobic core may be somewhat loose.

In examining other evidence for TFIIB conformational variability, we note the previous proposal that VP16ad disrupts an intramolecular interaction between the N-terminal and C-terminal domains of full-length TFIIB (37). This disruption may facilitate subsequent steps in PIC assembly by exposing TFIIB binding surfaces for TFIIF and RNAPII. We have examined the effects of VP16ad on ^{1}H−^{15}N HSQC spectra of full-length TFIIB, TFIIBc, and TFIIBn. VP16ad-induced reduction in line width and overlap of the ^{1}H−^{15}N HSQC spectrum of full-length TFIIB (Figure 3) is consistent with the proposed VP16ad disruption of a TFIIB intramolecular interaction (37): in full-length TFIIB, exchange between closed (N- and C-terminal domains in contact) and open conformations may contribute to the large line widths observed in the ^{1}H−^{15}N HSQC spectrum of TFIIB (Figure

3a); the spectrum in Figure 3b indicates that VP16ad binding may perturb the equilibrium to favor open TFIIB conformations with exposed interaction sites for TFIIF and RNAPII.

We next investigated the VP16ad binding site on TFIIB: our results suggest that VP16ad binds the first repeat of TFIIBc and either does not bind or does not significantly perturb the structure of TFIIBn. The distribution of chemical shift and line width changes in TFIIBc indicates that TFIIBn and VP16ad have the same or an overlapping binding surface on TFIIBc, suggesting that VP16ad and TFIIBn compete. Interestingly, competition between TAF$_{II}$250 and VP16ad for binding to TBP has been implicated as a mechanism of activation (72). Upon complexation of TFIIBc with either VP16ad or TFIIBn, we observed significant chemical shift and line width changes in numerous residues of the repeat−repeat interface and linker and in the hydrophobic core helix C1 (Figure 5). VP16ad-induced effects were more extensive than TFIIBn-induced effects. These results provide evidence for conformational changes in TFIIBc induced by either VP16ad or TFIIBn.

The combined relaxation and protein−protein interaction data suggest that TFIIB may exist in equilibrium between multiple conformational states, with intramolecular (or intermolecular) interaction between the N-terminal zinc binding and C-terminal core domains modulating the conformational equilibria. Transcriptional activators such as VP16 may similarly influence TFIIB conformation. In such a scenario, the solution structure of free TFIIBc represents a conformational state that may be less favorable in full-length TFIIB due to the presence of the N-terminal zinc binding domain.

Conformational changes in TFIIB are likely to have important consequences for transcriptional regulation. The rate-determining steps in transcription complex assembly depend on exact conditions, for example the concentration of each of the general factors. TFIIB binding to the TFIID−promoter complex can be a slow step. An activator may increase the rate of this step by inducing favorable conformational changes in TFIIB. Consistent with this notion, the equilibrium association constant for TFIIB binding to the

promoter can be increased by a single, promoter-bound activator (*73*). Although interaction with TBP results in greater structural ordering of VP16ad than interaction with TFIIB (*41*), our data indicate that VP16ad binding to TFIIBc exerts significant effects on TFIIBc backbone chemical shifts and line widths, particularly within the first repeat. It is also interesting that Roeder and colleagues proposed RNAPII-dependent conformational changes in TFIIB, analogous to those presumed for *E. coli* σ^{70} (*10*). In addition to TFIIB, it is likely that other general factors undergo conformational changes during PIC assembly (*4*) and other stages of the transcription cycle. The kinetics of TBP binding to the promoter, for example, are consistent with a two-step pathway involving initial binding followed by isomerization to a more stable complex (*74*). Also, studies of prokaryotic transcription initiation have lead to a model involving an isomerization step from a so-called closed to an open transcription complex (*75*).

Amino acid sequence comparison provides further circumstantial evidence for variability of TFIIB conformation. According to a published sequence alignment (*76*), both of the yeast TFIIBs that have been cloned and sequenced have insertions between the two repeats of the core domain relative to the higher eukaryotic TFIIB sequences: nine residues inserted on the N-terminal side of the interrepeat linker and three or five residues on the C-terminal side. This suggests that the two yeast TFIIBs have an interrepeat linker more than twice as long as higher eukaryotic TFIIBs, with concomitant potential for different relative orientation and/or spacing of the two repeats in the C-terminal core domain. This may be related to the position of the TATA motif in yeast, separated by 60−120 base pairs from the transcription initiation site compared to 35 base pairs in higher eukaryotes. It is also germane that the most highly conserved portion of TFIIB lies immediately C-terminal of the zinc binding motif, where there is 90% similarity over a 49-residue segment (*76*). This suggests that the sequence linking the zinc binding domain and the C-terminal core domain, and consequently the relative disposition of these domains, is important for function.

There are numerous other examples of multiple-domain proteins that show conformational variability with respect to domain orientations. The α subunit of *E. coli* RNA polymerase consists of two domains with different functions connected by a flexible linker (*77*). The characteristic dumbbell shape of calcium-loaded calmodulin collapses to a compact, globular form upon complexation with target peptide (*78−80*). Domain packing and the structure of the N-terminal domain of recoverin are very different between the X-ray crystal structure of unmyristoylated recoverin bound to a single calcium (*81*) and the NMR-derived solution structure of calcium-free myristoylated recoverin (*82*). Together with the present and previous (*37*) results, these observations lend weight to the notion that malleability in TFIIB domain organization plays a role in transcriptional regulation. In contrast, structurally related cyclin A is rigid and does not change conformation between free and CDK2-bound forms (*15, 83*).

CONCLUSIONS

The present data on TFIIBc dynamics and interactions are consistent with conformational fluctuations in TFIIBc.

Relatively large amplitude motions on the nanosecond time scale in the repeat−repeat linker indicate that this linking segment potentially acts as a hinge to permit reorientation of the two repeats. This possibility is supported by numerous TFIIBn- and VP16ad-induced changes in backbone NH chemical shift and line width in the linker and repeat−repeat interface of TFIIBc. The pattern of backbone NH chemical shift and line width changes indicates that VP16ad and TFIIBn bind primarily to the first repeat and that they compete for the same or overlapping binding sites on TFIIBc. TFIIB may exist in equilibrium between multiple conformations, with TFIIBn−TFIIBc interactions modulating the equilibria and with stabilization of the structure of isolated TFIIBc in the absence of the N-terminal zinc binding domain. Structural details of the 60-residue linker between the two domains remain to be elucidated. These observations suggest that transcriptional activators such as VP16 exert part of their effect by influencing TFIIB conformation to facilitate formation of the TFIIB−TBP−DNA complex.

REFERENCES

1. Conaway, R. C., and Conaway, J. W. (1993) *Annu. Rev. Biochem. 62*, 161−190.
2. Zawel, L., and Reinberg, D. (1995) *Annu. Rev. Biochem. 64*, 533−561.
3. Orphanides, G., Lagrange, T., and Reinberg, D. (1996) *Genes Dev. 10*, 2657−2683.
4. Roeder, R. G. (1996) *Trends Biochem. Sci. 21*, 327−335.
5. Buratowski, S., Hahn, S., Guarente, L., and Sharp, P. A. (1989) *Cell 56*, 549−561.
6. Lagrange, T., Kim, T. K., Orphanides, G., Ebright, Y. W., Ebright, R. H., and Reinberg, D. (1996) *Proc. Natl. Acad. Sci. U.S.A. 93*, 10620−10625.
7. Ha, I., Lane, W. S., and Reinberg, D. (1991) *Nature 352*, 689−695.
8. Malik, S., Hisatake, K., Sumimoto, H., Horikoshi, M., and Roeder, R. G. (1991) *Proc. Natl. Acad. Sci. U.S.A. 88*, 9553−9557.
9. Barberis, A., Muller, C. W., Harrison, S. C., and Ptashne, M. (1993) *Proc. Natl. Acad. Sci. U.S.A. 90*, 5628−5632.
10. Malik, S., Lee, D. K., and Roeder, R. G. (1993) *Mol. Cell. Biol. 13*, 6253−6259.
11. Bagby, S., Kim, S., Maldonado, E., Tong, K. I., Reinberg, D., and Ikura, M. (1995) *Cell 82*, 857−867.
12. Nikolov, D. B., Chen, H., Halay, E. D., Usheva, A. A., Hisatake, K., Lee, D. K., Roeder, R. G., and Burley, S. K. (1995) *Nature 377*, 119−128.
13. Kosa, P. F., Ghosh, G., DeDecker, B. S., and Sigler, P. B. (1997) *Proc. Natl. Acad. Sci. U.S.A. 94*, 6042−6047.
14. Brown, N. R., Noble, M. E., Endicott, J. A., Garman, E. F., Wakatsuki, S., Mitchell, E., Rasmussen, B., Hunt, T., and Johnson, L. N. (1995) *Structure 3*, 1235−1247.
15. Jeffrey, P. D., Russo, A. A., Polyak, K., Gibbs, E., Hurwitz, J., Massague, J., and Pavletich, N. P. (1995) *Nature 376*, 313−320.
16. Kim, K. K., Chamberlin, H. M., Morgan, D. O., and Kim, S.-H. (1996) *Nat. Struct. Biol. 3*, 849−855.
17. Andersen, G., Busso, D., Poterszman, A., Hwang, J. R., Wurtz, J.-M., Ripp, R., Thierry, J.-C., Egly, J.-M., and Moras, D. (1997) *EMBO J. 16*, 958−967.

18. Kim, H.-Y., and Cho, Y. (1997) *Nat. Struct. Biol. 4*, 390−395.

19. Gibson, T. J., Thompson, J. D., Blocker, A., and Kouzarides, T. (1994) *Nucleic Acids Res. 22*, 946−952.

20. Noble, M. E. M., Endicott, J. A., Brown, N. R., and Johnson, L. N. (1997) *Trends Biochem. Sci. 22*, 482−487.

21. Zhu, W., Zeng, Q., Colangelo, C. M., Lewis, M., Summers, M. F., and Scott, R. A. (1996) *Nat. Struct. Biol. 3*, 122−124.

22. Hori, R., and Carey, M. (1994) *Curr. Opin. Genet. Dev. 4*, 236−244.

23. Tjian, R., and Maniatis, T. (1994) *Cell 77*, 5−8.

24. Triezenberg, S. J. (1995) *Curr. Opin. Genet. Dev. 5*, 190−196.

25. Hanna-Rose, W., and Hansen, U. (1996) *Trends Genet. 12*, 229−234.

26. Johnson, A. D. (1995) *Cell 81*, 655−658.

27. Kaiser, K., and Meisterernst, M. (1996) *Trends Biochem. Sci. 21*, 342−345.

28. Kingston, R. E., Bunker, C. A., and Imbalzano, A. N. (1996) *Genes Dev. 10*, 905−920.

29. Krude, T., and Elgin, S. C. R. (1996) *Curr. Biol. 6*, 511−515.

30. Stringer, K. F., Ingles, C. J., and Greenblatt, J. (1990) *Nature 345*, 783−786.

31. Lin, Y. S., Ha, I., Maldonado, E., Reinberg, D., and Green, M. R. (1991) *Nature 353*, 569−571.

32. Xiao, H., Pearson, A., Coulombe, B., Truant, R., Zhang, S., Regier, J. L., Triezenberg, S. J., Reinberg, D., Flores, O., Ingles, C. J., and Greenblatt, J. (1994) *Mol. Cell. Biol. 14*, 7013−7024.

33. Triezenberg, S. J., Kingsbury, R. C., and McKnight, S. L. (1988) *Genes Dev. 2*, 718−729.

34. Regier, J. L., Shen, F., and Triezenberg, S. L. (1993) *Proc. Natl. Acad. Sci. U.S.A. 90*, 883−887.

35. Walker, S., Greaves, R., and O'Hare, P. (1993) *Mol. Cell. Biol. 13*, 5233−5244.

36. Roberts, S. G., Ha, I., Maldonado, E., Reinberg, D., and Green, M. R. (1993) *Nature 363*, 741−744.

37. Roberts, S. G., and Green, M. R. (1994) *Nature 371*, 717−720.

38. Roberts, S. G., Choy, B., Walker, S. S., Lin, Y. S., and Green, M. R. (1995) *Curr. Biol. 5*, 508−516.

39. Gupta, R., Emili, A., Pan, G., Xiao, H., Shales, M., Greenblatt, J., and Ingles, C. J. (1996) *Nucleic Acids Res. 24*, 2324−2330.

40. Chou, S., and Struhl, K. (1997) *Mol. Cell. Biol. 17*, 6794−6802.

41. Shen, F., Triezenberg, S. J., Hensley, P., Porter, D., and Knutson, J. R. (1996) *J. Biol. Chem. 271*, 4827−4837.

42. Tansey, W. P., and Herr, W. P. (1997) *Science 275*, 829−831.

43. Lee, M., and Struhl, K. (1997) *Mol. Cell. Biol. 17*, 1336−1345.

44. Ha, I., Roberts, S., Maldonado, E., Sun, X., Kim, L. U., Green, M., and Reinberg, D. (1993) *Genes Dev. 7*, 1021−1032.

45. Bagby, S., Tong, K. I., Liu, D., Alattia, J.-R., and Ikura, M. (1997) *J. Biomol. NMR 10*, 279−282.

46. Studier, F. W., and Moffatt, B. A. (1986) *J. Mol. Biol. 189*, 113−130.

47. Cavanagh, J., and Rance, M. (1990) *J. Magn. Reson. 88*, 72−85.

48. Palmer, A. G., III, Cavanagh, J., Wright, P. E., and Rance, M. (1991) *J. Magn. Reson. 93*, 151−170.

49. Kay, L. E., Keifer, P., and Saarinen, T. (1992) *J. Am. Chem. Soc. 114*, 10663−10665.

50. Muhandiram, D. R., and Kay, L. E. (1994) *J. Magn. Reson., Ser. B 103*, 203−216.

51. Grzesiek, S., and Bax, A. (1993) *J. Am. Chem. Soc. 115*, 12593−12594.

52. Li, Y.-C., and Montelione, G. T. (1993) *J. Magn. Reson., Ser. B 101*, 315−319.

53. Kay, L. E., Xu, G. Y., and Yamazaki, T. (1994) *J. Magn. Reson., Ser. A 109*, 129−133.

54. Stonehouse, J., Shaw, G. L., Keeler, J., and Laue, E. D. (1994) *J. Magn. Reson., Ser. A 107*, 178−184.

55. Farrow, N. A., Muhandiram, R., Singer, A. U., Pascal, S. M., Kay, C. M., Gish, G., Shoelson, S. E., Pawson, T., Forman-Kay, J. D., and Kay, L. E. (1994) *Biochemistry 33*, 5984−6003.

56. Farrow, N. A., Zhang, O., Szabo, A., Torchia, D. A., and Kay, L. E. (1995) *J. Biomol. NMR 6*, 153−162.

57. Phan, I. Q. H., Boyd, J., and Campbell, I. D. (1996) *J. Biomol. NMR 8*, 369−378.

58. Tjandra, N., Kuboniwa, H., Ren, H., and Bax, A. (1995) *Eur. J. Biochem. 230*, 1014−1024.

59. Delaglio, F., Grzesiek, S., Vuister, G. W., Zhu, G., Pfeifer, J., and Bax, A. (1995) *J. Biomol. NMR 6*, 277−293.

60. Garrett, D. S., Powers, R., Gronenborn, A. M., and Clore, G. M. (1991) *J. Magn. Reson. 95*, 214−220.

61. Palmer, A. G., III, Rance, M., and Wright, P. E. (1991) *J. Am. Chem. Soc. 113*, 4371−4380.

62. Stone, M. J., Fairbrother, W. J., Palmer, A. G., III, Reizer, J., Saier, M. H., Jr., and Wright, P. E. (1992) *Biochemistry 31*, 4394−4406.

63. Lipari, G., and Szabo, A. (1982) *J. Am. Chem. Soc. 104*, 4546−4559.

64. Lipari, G., and Szabo, A. (1982) *J. Am. Chem. Soc. 104*, 4559−4570.

65. Yamasaki, K., Saito, M., Oobatake, M., and Kanaya, S. (1995) *Biochemistry 34*, 6587−6601.

66. Kay, L. E., Torchia, D. A., and Bax, A. (1989) *Biochemistry 28*, 8972−8979.

67. Ishima, R., and Nagayama, K. (1995) *Biochemistry 34*, 3162−3171.

68. Peng, J. W., and Wagner, G. (1995) *Biochemistry 34*, 16733−16752.

69. Farrow, N. A., Zhang, O., Forman-Kay, J. D., and Kay, L. E. (1995) *Biochemistry 34*, 868−878.

70. Zhang, O., and Forman-Kay, J. D. (1995) *Biochemistry 34*, 6784−6794.

71. Cheng, J.-W., Lepre, C. A., Chambers, S. P., Fulghum, J. R., Thomson, J. A., and Moore, J. M. (1993) *Biochemistry 32*, 9000−9010.

72. Nishikawa, J., Kokubo, T., Horikoshi, M., Roeder, R. G., and Nakatani, Y. (1997) *Proc. Natl. Acad. Sci. U.S.A. 94*, 85−90.

73. Choy, B., and Green, M. R. (1993) *Nature 366*, 531−536.

74. Hoopes, B. C., LeBlanc, J. F., and Hawley, D. K. (1992) *J. Biol. Chem. 267*, 11539−11547.

75. McClure, W. R. (1985) *Annu. Rev. Biochem. 54*, 171−204.

76. Na, J. G., and Hampsey, M. (1993) *Nucleic Acids Res. 21*, 3413−3417.

77. Jeon, Y. H., Yamazaki, T., Otomo, T., Ishihama, A., and Kyogoku, Y. (1997) *J. Mol. Biol. 267*, 953−962.

78. Ikura, M., Clore, G. M., Gronenborn, A. M., Zhu, G., Klee, C. B., and Bax, A. (1992) *Science 256*, 632−638.

79. Meador, W. E., Means, A. R., and Quiocho, F. A. (1992) *Science 257*, 1251−1255.

80. Meador, W. E., Means, A. R., and Quiocho, F. A. (1993) *Science 262*, 1718−1721.

81. Flaherty, K. M., Zozulya, S., Stryer, L., and McKay, D. B. (1993) *Cell 75*, 709−716.

82. Tanaka, T., Ames, J. B., Harvey, T. S., Stryer, L., and Ikura, M. (1995) *Nature 376*, 444−447.

83. Russo, A., Jeffrey, P. D., and Pavletich, N. P. (1996) *Nat. Struct. Biol. 3*, 696−700.

84. Lagrange, T., Kapanidis, A. N., Tang, H., Reinberg, D., and Ebright, R. H. (1998) *Genes Dev. 12*, 34−44.